Nonlinear Dynamics **26:** 253–271, 2001.

Distinguishing Periodic and Chaotic Time Series Obtained from an Experimental Nonlinear Pendulum

L. F. P. FRANCA and M. A. SAVI
Department of Mechanical and Materials Engineering, Military Institute of Engineering, 22.290.270 Rio de Janeiro, Brazil

(Received: 31 May 2000; accepted: 16 February 2001)

Abstract. The experimental analysis of nonlinear dynamical systems furnishes a scalar sequence of measurements, which may be analyzed using state space reconstruction and other techniques related to nonlinear analysis. The noise contamination is unavoidable in cases of data acquisition and, therefore, it is important to recognize techniques that can be employed for a correct identification of chaos. The present contribution discusses the experimental analysis of a nonlinear pendulum, considering state space reconstruction, frequency domain analysis and the determination of dynamical invariants, Lyapunov exponents and attractor dimension. A procedure to construct Poincaré map of the signal is presented. The analyses of periodic and chaotic motions are carried out in order to establish a difference between them. Results show that it is possible to distinguish periodic and chaotic time series obtained from an experimental set up employing proper procedures even though noise suppression is not contemplated.

Keywords: Chaos, nonlinear dynamics, nonlinear pendulum, experimental analysis.

1. Introduction

The experimental analysis of nonlinear dynamical systems furnishes a scalar sequence of measurements. Therefore, a time series associated with system dynamics is available, being interesting to analyze it using state space reconstruction and other techniques related to nonlinear analysis. The noise contamination is unavoidable in cases of data acquisition and noise suppression is essential in signal processing, especially in chaos analysis. Many studies are devoted to evaluate noise suppression and its effects in the analysis of chaos [1–5]. However, there are a small number of reports devoted to the effects of the system noise on chaos [1].

The analysis of nonlinear dynamical systems from time series involves state space reconstruction. Basically, there are two different methods for this aim: derivative coordinates and delay coordinates [6–8]. The method of delay coordinates has proven to be a powerful tool to analyze chaotic behavior of dynamical system. Ruelle [9], Packard et al. [6] and Takens [7] introduced the basic idea of this method and the main problem arising is the determination of the embedding parameters.

Nonlinear analysis also involves the determination of quantities, known as dynamical invariants, which are important to identify chaotic behavior. Lyapunov exponents and attractor dimension are some examples. Lyapunov exponents evaluate the sensitive dependence to initial conditions estimating the exponential divergence of nearby orbits. These exponents have been used as the most useful dynamical diagnostic tool for chaotic system analysis. The signs of the Lyapunov exponents provide a qualitative picture of the system's dynamics and any system containing at least one positive exponent presents chaotic behavior. The determination

of Lyapunov exponents of dynamical system with an explicitly mathematical model, which can be linearized, is well established from the algorithm proposed by Wolf et al. [10]. On the other hand, the determination of these exponents from time series is quite more complex. Basically, there are two different classes of algorithms: Trajectories, real space or direct method [10–12]; and perturbation, tangent space or Jacobian matrix method [13–20].

The attractor dimension counts the effective number of degrees of freedom in the dynamical system. The strangeness of the chaotic attractor is associated with its dimension in which instance it is described by a noninteger dimension. There are a variety of different forms to define or quantify the dimension of an attractor. Farmer et al. [21] presents an overview of these definitions, considering two general types: those that depend only on metric properties and those that depend on the frequency with which a typical trajectory visits different regions of the attractor. Furthermore, there is the Kaplan–Yorke conjecture that defines the Lyapunov dimension calculated from Lyapunov exponents.

The main purpose of this contribution is to present proper procedures which are capable to distinguish periodic and chaotic signals obtained from an experimental nonlinear pendulum. Noise suppression is not contemplated and the signal is analyzed without filtering. State space reconstruction, frequency domain analysis and the determination of dynamical invariants, Lyapunov exponents and attractor dimension, are considered. Furthermore, it is necessary to present a procedure to construct a Poincaré map of the signal, which is also discussed. The choice of algorithms to be employed is based on the analysis of noise sensitivity developed in [22–24]. Algorithms proposed by Kantz [11] and by Rosenstein et al. [12] are conceived to estimate Lyapunov exponents. The use of these algorithms implies the determination of parameters before performing signal analysis. A calibration procedure is employed in order to define these parameters, which may be used for all signals, allowing their correct identification. Concerning to the attractor dimension, the algorithm due to Hegger et al. [25] to estimate correlation dimension is employed. Results show that it is possible to distinguish periodic and chaotic signals even though noise suppression is not contemplated. The authors agree that these procedures can be employed to other dynamical systems.

2. Nonlinear Analysis

This section presents a brief overview of the main techniques employed in nonlinear time series analysis [26–29]. Linear signal processing, state space reconstruction and the evaluation of dynamical invariants, Lyapunov exponents and attractor dimension, are discussed.

2.1. Linear Signal Processing

The most common and very useful way of analyzing a time series using linear signal processing techniques is to construct the power spectrum and its Fast Fourier Transform (FFT) [29]. As it is well known, the FFT of a chaotic signal presents continuous spectra over a limited range and the energy is spread over a wider bandwidth. On the other hand, FFT of a periodic signal presents discrete spectra, where a finite number of frequencies contribute for the response [29, 30]. Another useful measure that can be employed in the signal analysis is the autocorrelation function [29].

One of the clues to detecting chaos is the appearance of a broad spectrum of frequencies in the output when the input is a single-frequency harmonic motion. Therefore, even though these techniques are very useful, one must be cautioned on their application. In large degrees

of freedom systems, for example, the use of the Fourier spectrum may not be of much help in detecting chaos [30]. Hence, in many situations it may become difficult to distinguish noise and chaos. This contribution considers the FFT as the first step on the analysis of experimental signals.

2.2. State Space Reconstruction

The basic idea of the state space reconstruction is that a signal contains information about unobserved state variables which can be used to predict the present state. Therefore, a scalar time series, $s(t)$, may be used to construct a vector time series that is equivalent to the original dynamics from a topological point of view. The state space reconstruction needs to form a coordinate system to capture the structure of orbits in state space which could be done using lagged variables, $s(t+\tau)$, where τ is the time delay. Then, considering an experimental signal, $s(n)$, $n = 1, 2, 3, \ldots, N$, where $t = t_0 + (n-1)\Delta t$, it is possible to use a collection of time delays to create a vector in a D_e-dimensional space,

$$u(t) = \{s(t), s(t+\tau), \ldots, s(t+(D_e-1)\tau\}^T. \tag{1}$$

The method of delays has become popular for dynamical reconstruction, however, the choice of the delay parameters, τ (time delay) and D_e (embedding dimension) has not been fully developed. Many researches have been developed considering the better approaches to estimate delay parameters for different kinds of time series.

The literature reports many methods employed to determine time delay. The global singular value method [8] and the autocorrelation function [31] are some examples. Nevertheless, the mutual information method [32] presents better results, which disseminate its use.

The determination of embedding dimension, D_e, involves four different methods: the saturation with dimension of system invariants [33]; the singular value decomposition (SVD) [8]; the false nearest neighbors (FNN) [34]; and the true vector fields [35]. Recently, the method of averaged false neighbors (AFN) [36] and the method of false strand neighbors (FSN) [37] are proposed as improvements of the FNN taking into account noise signals.

Since Franca and Savi [22–24] show that the average mutual information method and the method of false nearest neighbors has no noise sensitivity, this contribution uses them in order to determine the time delay and the embedding dimension, respectively.

2.2.1. *Method of Mutual Information*

Fraser and Swinney [32] establishes that the time delay τ corresponds to the first local minimum of the average mutual information function $I(\tau)$, which is defined as follows:

$$I(\tau) = \sum \Gamma_b(s(t), s(t+\tau)) \log_2 \left[\frac{\Gamma_b(s(t), s(t+\tau))}{\Gamma_b(s(t))\Gamma_b(s(t+\tau))} \right], \tag{2}$$

where $\Gamma_b(s(t))$ is the probability of the measure $s(t)$, $\Gamma_b(s(t+\tau))$ is the probability of the measure $s(t+\tau)$, and $\Gamma_b(s(t), s(t+\tau))$ is the joint probability of the measure of $s(t)$ and $s(t+\tau)$ [32]. The average mutual information is really a kind of generalization to the nonlinear phenomena from the correlation function in the linear phenomena. When the measures $s(t)$ and $s(t+\tau)$ are completely independent, $I(\tau) = 0$. On the other hand, when $s(t)$ and $s(t+\tau)$ are equal, $I(\tau)$ is maximum. Therefore, plotting $I(\tau)$ *versus* τ makes it possible to identify the best value for the time delay which is related to the first local minimum.

2.2.2. *Method of False Nearest Neighbors*

The FNN algorithm was originally developed for determining the number of time delay coordinates needed to recreate autonomous dynamics, but it is extended to examine the problem of determining the proper embedding dimension.

In an embedding dimension that is too small to unfold the attractor, not all points that lie close to one another will be neighbors because of the dynamics. Some will actually be far from each other and simply appear as neighbors because the geometric structure of the attractor has been projected down onto a smaller space [34].

In order to consider the method of FFN, a D-dimensional space is conceived where the point $u(t)$ has rth nearest neighbors, $u^{(r)}(t)$. The square of the Euclidean distance between these points is

$$r_D^2(t,r) = \sum_{k=0}^{D-1} [s(t+k\tau) - s^{(r)}(t+k\tau)]^2. \tag{3}$$

Now, going from dimension D to $D+1$ by time delay, there is a new coordinate system and, as a consequence, a new distance between $u(t)$ and $u^{(r)}(t)$. When these distances alter from one dimension to another, there are false neighbors. A natural criterion for catching embedding errors is that the increase in distance between $u(t)$ and $u^{(r)}(t)$ is large when going from dimension D to $D+1$. The increase in distance can be stated with distance equations and some criteria must be established to designate the existence of false neighbors. Kennel et al. [34] established proper criteria for this aim.

2.3. Lyapunov Exponents

Lyapunov exponents evaluate the sensitive dependence to initial conditions considering the exponential divergence of nearby orbits. Therefore, it is necessary to evaluate how trajectories with nearby initial conditions diverge. The dynamics of the system transforms the D-sphere of states in a D-ellipsoid and, mathematically, the Lyapunov exponents considers $d(t) = d_0 b^{\lambda t}$, where b is a reference basis. The signs of the Lyapunov exponents provide a qualitative picture of the system's dynamics. The existence of positive Lyapunov exponents defines directions of local instabilities in the system dynamics.

The determination of Lyapunov exponents of dynamical system with an explicitly mathematical model, which can be linearized, is well established from the algorithm proposed by Wolf et al. [10]. On the other hand, the determination of these exponents from time series is quite more complex. Basically, there are two different classes of algorithms: trajectories, real space or direct method [10–12]; and perturbation, tangent space or Jacobian matrix method [13–20].

Franca and Savi [22–24] show that the algorithms due to Kantz [11] and due to Rosenstein et al. [12] allow one to establish a difference between periodic and chaotic motion, presenting no noise sensitivity. Hence, this contribution considers these algorithms in order to estimate Lyapunov exponents.

The algorithm proposed by Kantz [11] uses the same idea of the one proposed by Wolf et al. [10] which considers the reconstructed attractor and examines orbital divergence on length scales, working in tangent space. The method monitors the long-term evolution of a single pair of nearby orbits and is able to estimate the non-negative Lyapunov exponents. In principle, this method allows one to compute all Lyapunov spectrum but in reality it is limited to the

maximum one [11]. Kantz [11] considers that the divergence rate trajectories fluctuates along the trajectory, with the fluctuation given by the spectrum of effective Lyapunov exponents. The average of effective Lyapunov exponent along the trajectory is the true Lyapunov exponent and the maximum value is given by

$$\lambda(t) = \lim_{\varepsilon \to \infty} \frac{1}{\delta} \ln \left(\frac{|u(t+\delta) - u_\varepsilon(t+\delta)|}{\varepsilon} \right), \tag{4}$$

where $|u(0) - u_\varepsilon(0)| = \varepsilon$ and $u(t) - u_\varepsilon(t) = \varepsilon v_u(t)$, with $v_u(t)$ representing the eigenvectors associated with the maximum Lyapunov exponent, $\lambda_{\max}$; δ is a relative time referring to the time index of the point where the distance begin to be greater than ε, $\delta(0)$.

Rosenstein et al. [12] proposed a similar algorithm where the distance between the trajectories is defined as the Euclidean norm in the reconstructed phase space and, also, they have used only one neighbor trajectory.

2.4. Attractor Dimension

There are a variety of different forms to define or quantify the dimension of an attractor. Farmer et al. [21] presents an overview of these definitions, considering two general types: those that depend only on metric properties and those that depend on the frequency with which a typical trajectory visits different regions of the attractor. Furthermore, there is the Kaplan–Yorke conjecture that defines the Lyapunov dimension calculated from Lyapunov exponents.

Regarding the conclusions in [22–24], this contribution considers the correlation dimension employing the algorithm discussed by Hegger et al. [23], based on the Theiler's algorithm [38]. The correlation dimension, D_C, represents one of the most popular forms to measure the dimension of the attractor. This measure has been successfully used by many experimentalists and is defined as follows [30]:

$$D_C = \lim_{\varepsilon \to 0} \frac{-\log \sum_i \Gamma_i^2(\varepsilon)}{\log \varepsilon}, \tag{5}$$

where Γ_i is a correlation function of two points. Grassberger and Proccacia [33] and Takens [39] suggest the use of the correlation integral, $C(\varepsilon, N)$, to estimate $\sum_i \Gamma_i^2$. The popularity of the correlation algorithm is based on its straightforward implementation.

3. Experimental Apparatus

The experimental data related to the nonlinear pendulum response is obtained from the apparatus depicted in Figure 1. The pendulum is constructed by a disc with a lumped mass (1) and is connected to a rotary motion sensor (3). The dissipation is provided by a magnetic device (2), which is adjustable. A motor-string-spring device (4, 5) provides the excitation for the pendulum. The motor (5), PASCO ME-8750, has the following characteristics: 12 V DC, 0.3–3 Hz and 0–0.3 A. The signal measurement is done with the aid of two transducers. The rotary motion sensor (3), PASCO encoder CI-6538, has 1440 orifices and a precision of 0.25°. The magnetic transducer (6) is employed in order to generate a frequency signal associated with the forcing frequency of the motor, which is used to construct the Poincaré map of the signal. The apparatus is connected with an A/D interface, Science Workshop Interface 500 (CI-6760) where the sampling frequency varies from 2 Hz to 20 kHz. The interface oversamples the signal 8 times for frequencies below 100 Hz and a single time for higher sampling rates.

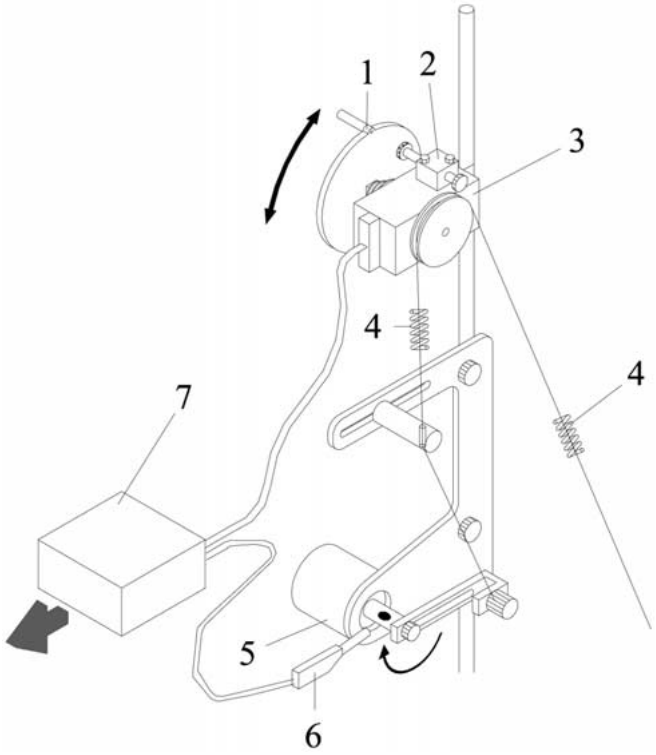

Figure 1. Experimental apparatus of the nonlinear pendulum: (1) disc with lumped mass; (2) magnetic damping device; (3) rotary motion sensor: PASCO CI-6538; (4) spring; (5) DC Motor: PASCO ME-8750; (6) magnetic transducer: TEKTRONIX; (7) Science Workshop interface: PASCO CI-6760.

Furthermore, this interface does not have any anti-aliasing filters and a 9 V AC-DC adapter provides power supply.

All signals are analyzed with the aid of the Science Workshop Data Acquisition, which allows one to evaluate angular velocity ($y = \dot{\theta}$) and angular position ($x = \theta$). Noise suppression is not contemplated and all signals are stored without filtering.

In order to perform the analysis of the nonlinear pendulum, one conceives that the time series is a sequence of angular position measured from the experiment, $s = x = \theta$. The apparatus also permits to measure the angular velocity $y = \dot{\theta}$, which is used to construct the real phase space (x *versus* y), employed to perform a visual validation of the reconstructed phase space.

3.1. Identification of System Parameters

Some characteristics of the apparatus are now discussed in order to identify the parameters of the pendulum. At first, the 12 V DC motor is considered. Figure 2 shows the frequency (Ω_e) *versus* voltage curve which is important to identify the forcing frequency of the system. Other important parameter that needs to be quantified is the dissipation, related to a magnetic damping device. A convenient procedure is the logarithmic decrement [40], which is defined verifying the ratio between any two consecutive displacement amplitudes. The analysis of this definition yields

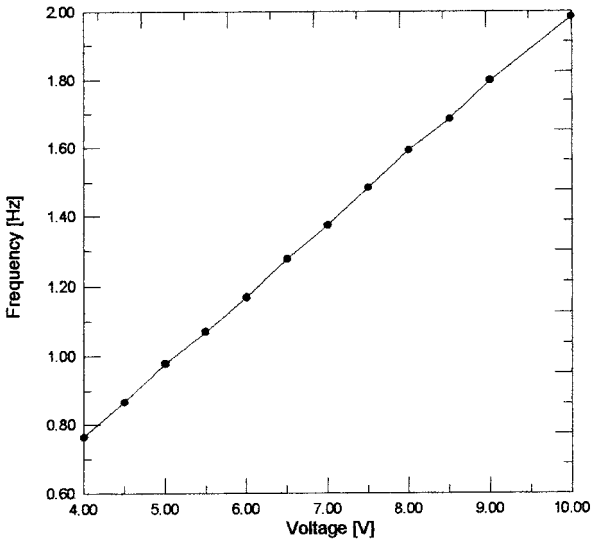

Figure 2. Identification of forcing frequency *versus* motor voltage.

$$\gamma = \frac{1}{j} \ln \frac{h_1}{h_{j+1}}, \tag{6}$$

where h_1 and h_{j+1} are the amplitude of the displacements at time instants t_1 and $t_{j+1} = t_1 + jT_d$, respectively, with j being an integer number and $T_d = 2\pi/\omega_d$; ω_d is the free damping frequency. Under these assumptions, the non-dimensional viscous damping parameter, ς, is defined as follows:

$$\varsigma = \frac{\gamma}{\sqrt{(2\pi) + \gamma^2}}. \tag{7}$$

3.2. Poincaré Maps

The Poincaré map is an important tool to observe the response of a nonlinear system. Experimentally, this can be done in several ways. Moon [30] presents a procedure employing a signal converter that stores the sampled data in a computer for display at a later time. Here, similar procedure is conceived in order to generate two signals: one associated with the motion and the other associated with the forcing frequency. The forcing frequency signal is generated with the aid of a magnetic transducer, which induces electric pulses when a reference bolt, connected to the motor, passes near it. These pulses are compared with the motion signal in order to generate a third signal representing the Poincaré Map where only measures in these time instants are contemplated.

4. Periodic Signal

In order to analyze a periodic response of the experimental nonlinear pendulum, a period-2 signal is considered with $N = 38{,}090$ points, generated with a motor voltage $V = 4.2$ V ($\Omega_e = 0.82$ Hz), a sample frequency $\Omega_s = 20$ Hz and a damping parameter $\varsigma = 0.0065$. The time history evolution of part of the signal is presented in Figure 3.

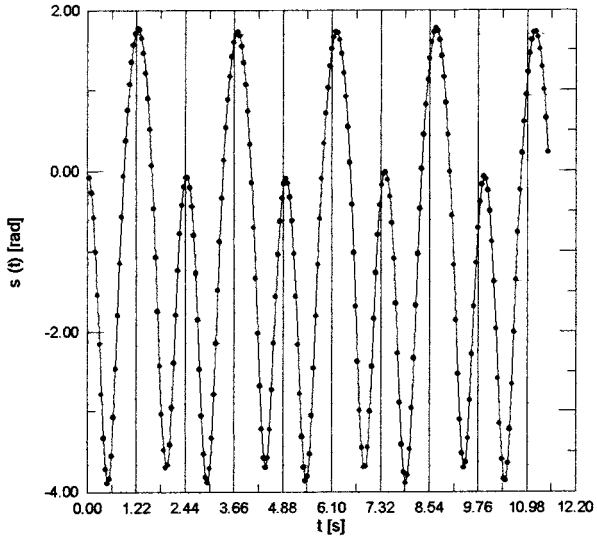

Figure 3. Periodic signal.

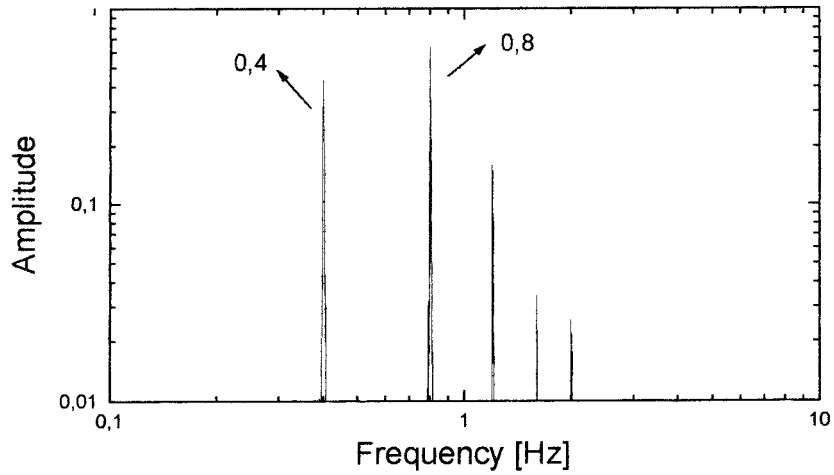

Figure 4. FFT of the periodic signal.

The analysis begins with the FFT spectrum, presented in Figure 4. This FFT shows a discrete spectrum where two fundamental frequencies are noticeable: the forcing frequency, $\Omega_e = 0.8$ Hz, and also 0.4 Hz. This evidences a period-2 motion, confirming the time history presented in Figure 3. The next step of the analysis is the state space reconstruction.

4.1. State Space Reconstruction

The state space reconstruction considers the signal derived from experiment to form a coordinate system that captures the structure of orbits in state space. This contribution employs the method of delay coordinates and, therefore, it is necessary to determine delay parameters, τ and D_e. Results of the analysis for the determination of these parameters is presented in Figure 5. Figure 5a shows the mutual information *versus* time delay, and the first minimum

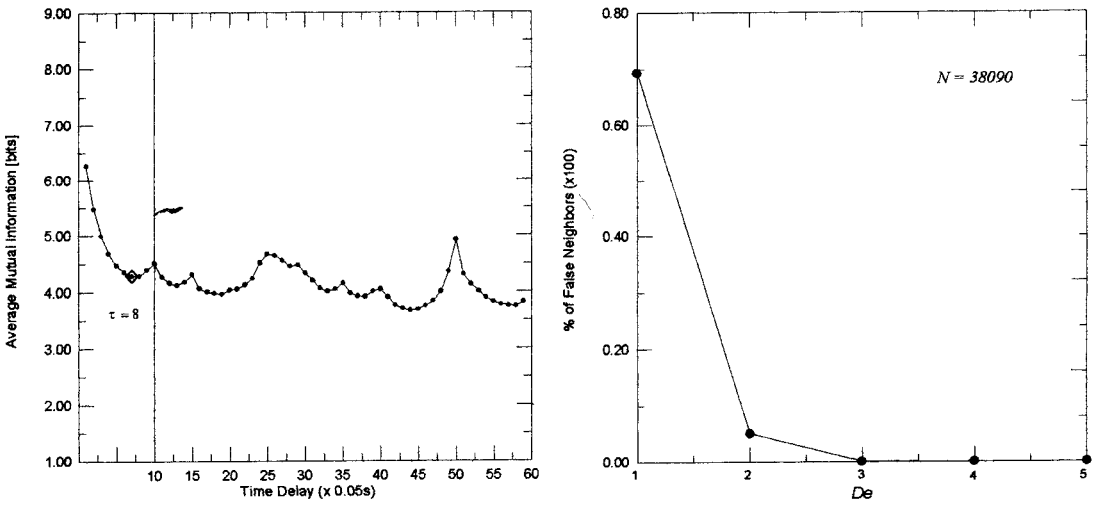

Figure 5. Delay parameters associated with periodic signal. (a) Average mutual information *versus* τ; (b) percentage of false neighbors *versus* D_e.

of this curve defines the time delay, $\tau = 8 \times 0.05 = 0.40$ s. Figure 5b presents the curve of the percentage of false neighbor points *versus* embedding dimension, indicating that the embedding dimension needs to be between 3 and 4.

After the determination of delay parameters, state space can be reconstructed. Figures 6a and 6b present the reconstructed phase space projected in dimension 2 and 3 while Figure 6c presents the real phase space measured in the experiment. Both spaces are similar from a topological point of view [7], presenting just a small coordinate change from one to another. Noise does not have a significantly influence in the determination of delay parameters. Notice that the reconstructed phase space presents a closed curve that is typical of periodic motions. In order to construct a Poincaré map of the motion, two signals are considered: one associated with the motion and the other associated with the forcing frequency. The Poincaré map defined by this procedure is presented in Figure 7. Figure 7a presents the reconstructed Poincaré section while Figure 7b the phase space, also pointing the Poincaré section. Notice that the Poincaré section shows two clouds of points, representing a period-2 motion. This result can be used to evaluate the noise level on data acquisition since only two points was expected. Therefore, the length of the range around each point is associated with noise.

4.2. Dynamical Invariants

Even though the system response presents a periodic-like characteristic, it is important to assure this conclusion with the determination of dynamical invariants. At first, Lyapunov exponents are focused. Since the greater exponent is the most important to diagnose chaotic motion, and taking into account the conclusions about noise sensitivity presented in [22–24], algorithms proposed by Kantz [11] and by Rosenstein et al. [12] are conceived. The analysis is done regarding the Poincaré map of the signal. The use of these algorithms implies the determination of parameter ε before performing signal analysis. In order to 'calibrate' the algorithm, a known signal is analyzed, for example a simple periodic motion, defining the

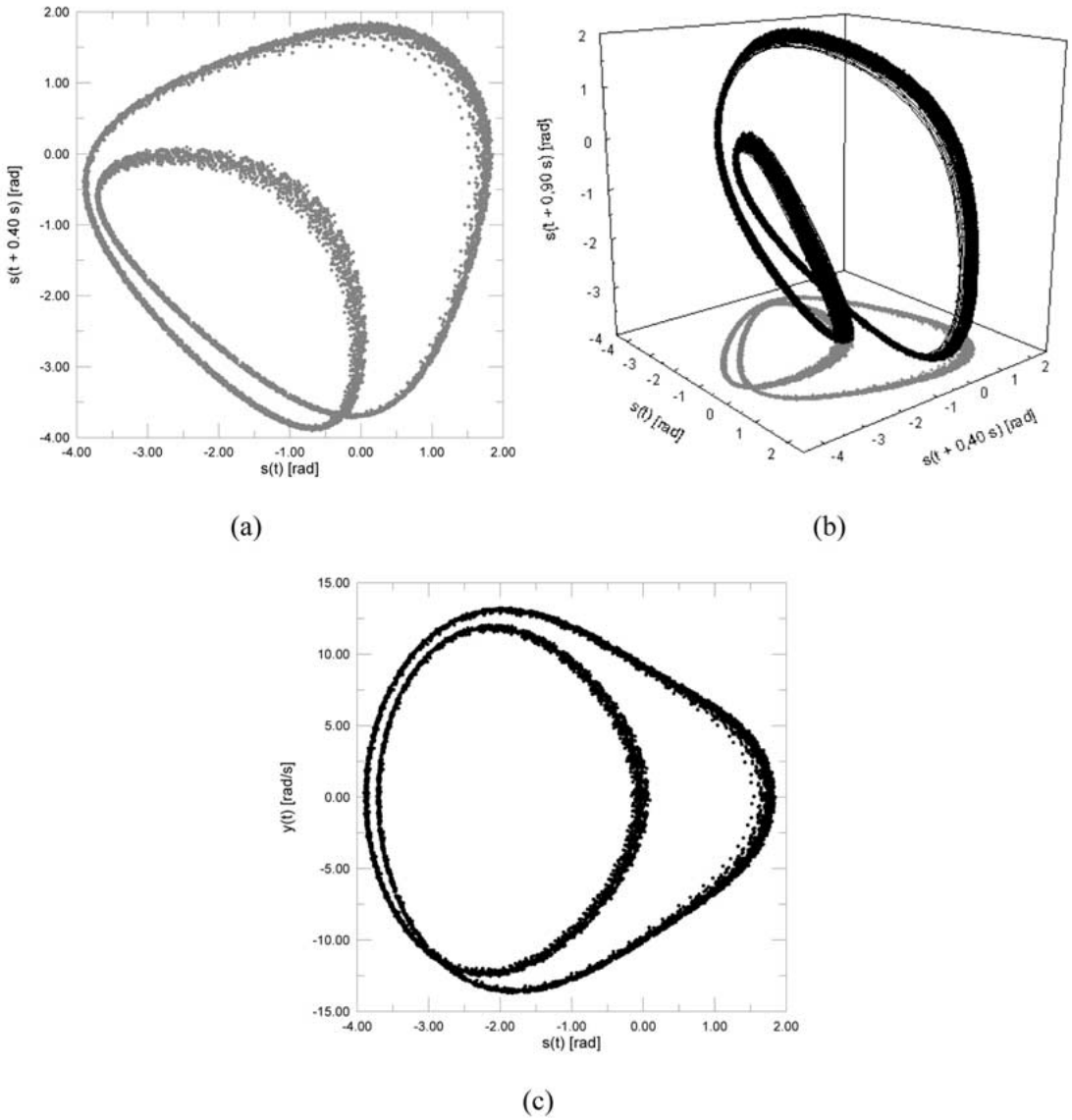

Figure 6. State space associated with periodic signal. (a) Reconstructed, 2-Dim; (b) Reconstructed, 3-Dim; (c) real.

correct value of this parameter. After this calibration, the parameter may be employed for all signals, allowing their correct identification.

Figure 8a presents the curve $S(\delta)$ *versus* predicted by the algorithm due to Kantz using $\varepsilon = 1.6$ and $D_e = 3, 6, 9, 12$. This curve has a null slope, meaning that $\lambda_{\max} = 0$, and therefore, the signal is related to a periodic motion. On the other hand, Figure 8b presents the curve $S(\delta)$ *versus* δ predicted by the algorithm due to Rosenstein et al. for the same parameters. In this case, the curve presents a non-null slope, which indicates a positive exponent.

The difference between both algorithms is, perhaps, associated with the use of only one neighbor per time on the algorithm due to Rosenstein et al., and not all neighbors within a certain neighborhood, which might induce larger statistical errors, especially in the presence

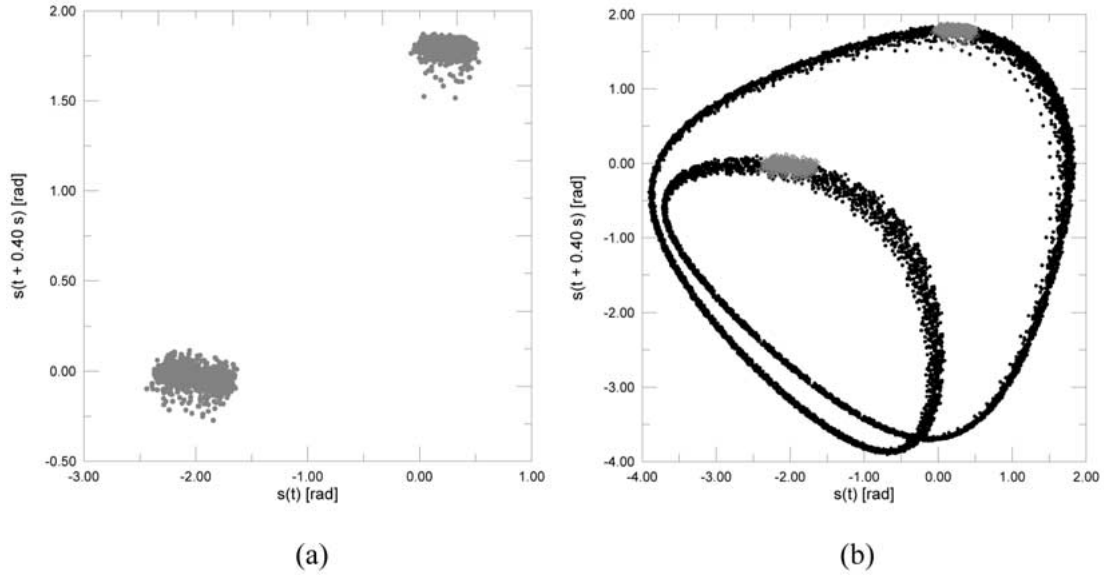

Figure 7. Poincaré map associated with periodic signal: (a) reconstructed; (b) phase space.

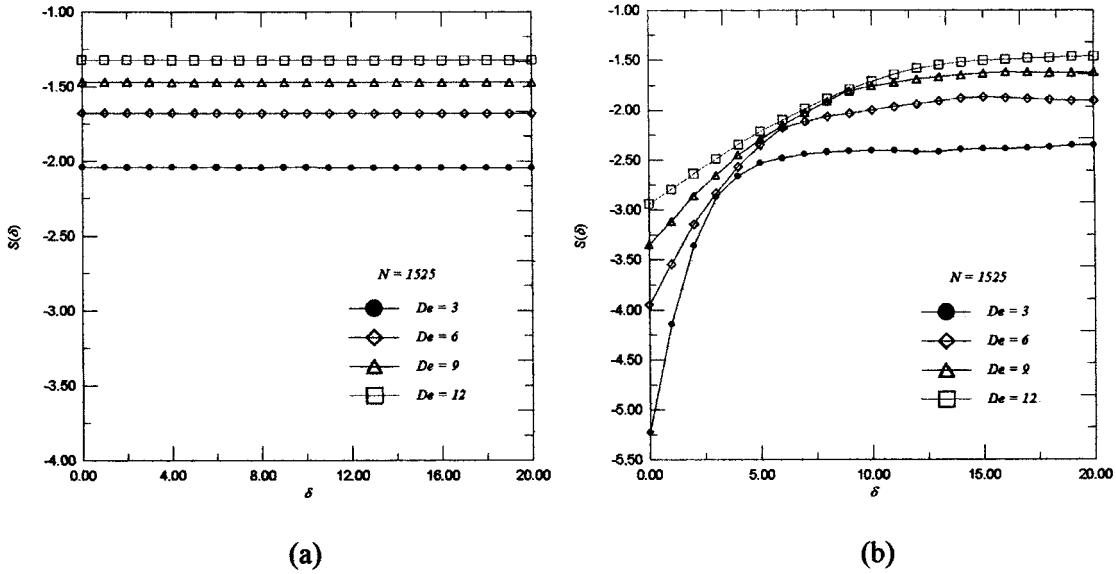

Figure 8. Lyapunov exponents associated with periodic signal. (a) Kantz; (b) Rosenstein et al.

of noise. This problem was pointed by Kantz [11] and may explain different results obtained by both methods.

At this point, the attractor dimension is in order. Hence, the continuous signal is regarded to determine the correlation dimension employing the algorithm due to Hegger et al. [23]. The correlation dimension for different values of embedding dimension is presented in Figure 9. The slope of the linear range in Figure 9a is related to the position of the horizontal range in Figure 9b and represents the measure of the correlation dimension. The value estimated for the correlation dimension belongs to the range 1.05 to 1.18. Notice that the inferior limit is close to 1, which is the expected value for this signal. Nevertheless, this range includes

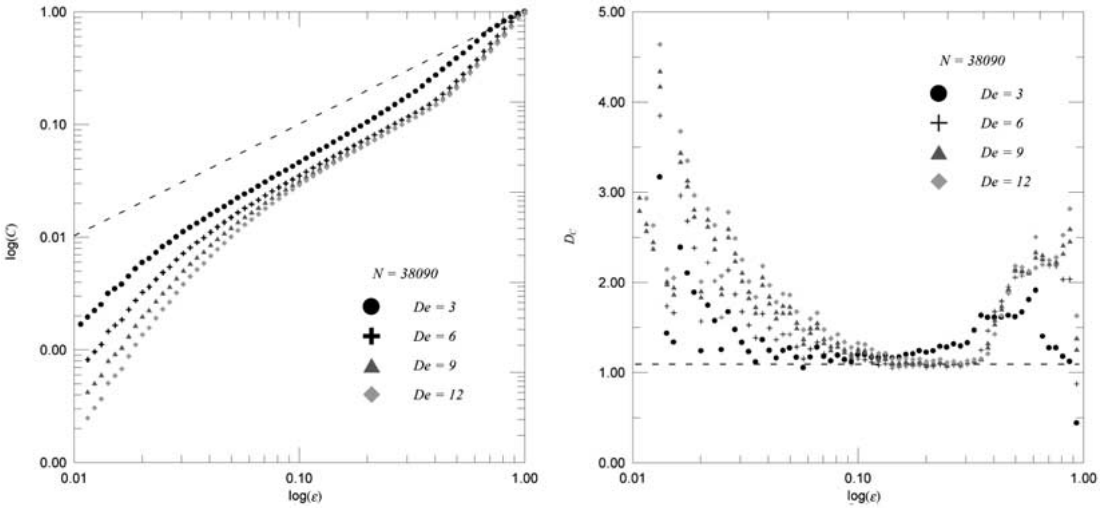

Figure 9. Correlation dimension associated with periodic signal. (a) $\log C(\varepsilon)$ *versus* $\log(\varepsilon)$; (b) $\log D_c$ *versus* $\log(\varepsilon)$.

noninteger numbers, which introduces difficulties in characterizing the motion. Another problem is related to the embedding dimension dependence, which also introduces difficulties to the correct estimation of the attractor dimension. Therefore, the attractor dimension is not an efficient criterion to identify a periodic signal.

5. Chaotic Signal

Chaos in the experimental nonlinear pendulum is analyzed considering a chaotic signal with $N = 30{,}589$ points, generated with a motor voltage $V = 4.2$ V ($\Omega_e = 0.82$ Hz), a sample frequency $\Omega_s = 20$ Hz and a damping parameter $\varsigma = 0.0125$. The time history evolution of part of the signal is shown in Figure 10.

Using the FFT, it is possible to see that the fundamental frequency $\Omega_e = 0.8$ Hz is immersed in a continuous spectrum of frequencies (Figure 11). This behavior is typical of chaotic motion, nevertheless it must be confirmed determining dynamical invariants. The following section reports on the state space reconstruction.

5.1. State Space Reconstruction

The state space reconstruction from the experimental signal employing the method of delay coordinates is now in focus. Results of the analysis employed to determine the delay parameters are presented in Figure 12. Figure 12a shows the mutual information *versus* time delay, and the first minimum of the curve must be used as the time delay, furnishing $\tau = 6 \times 0.05 = 0.30$ s. Figure 12b presents the curve of the percentage of false neighbor points *versus* embedding dimension, showing that the embedding dimension needs to be between 3 and 4. This result is in agreement with the one obtained for the periodic signal.

After the determination of delay parameters, it is possible to reconstruct state space. Figures 13a and 13b present the reconstructed phase space projected in dimension 2 and 3 while

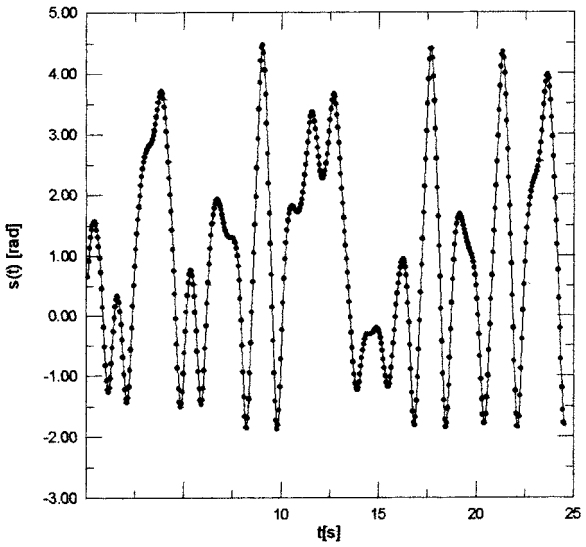

Figure 10. Chaotic signal.

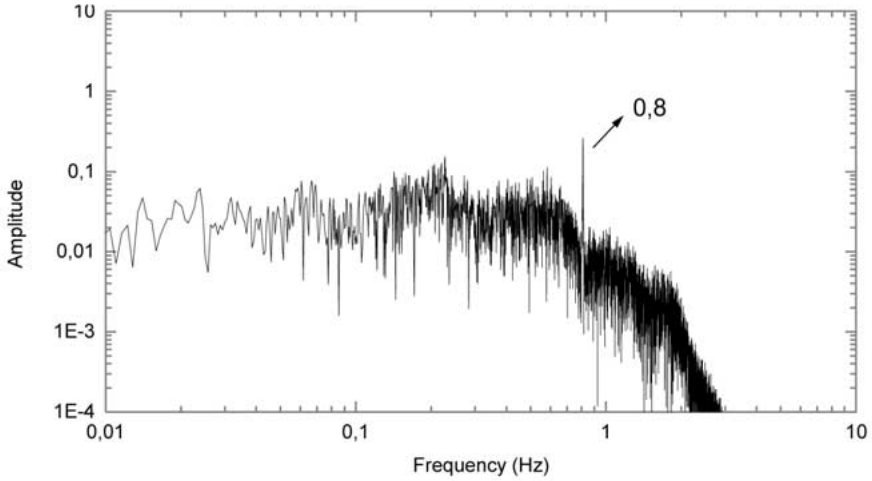

Figure 11. FFT of the chaotic signal.

Figure 13c presents the real phase space measured in the experiment. Both spaces are similar from a topological point of view [7], presenting just a small coordinate change from one to another. Once again, noise does not have a significantly influence in the determination of delay parameters. Here, phase space presents a chaotic-like characteristic because the orbit is not a closed curve.

In order to construct the Poincaré map of the chaotic signal, the same procedure used in the preceding section is employed. The Poincaré map defined by this procedure is presented in Figure 14. Figure 14a shows the reconstructed Poincaré section while Figure 14b shows the real one. A strange attractor is clearly identified presenting a fractal-like structure. Nevertheless, it is useful to confirm this with the calculation of dynamical invariants.

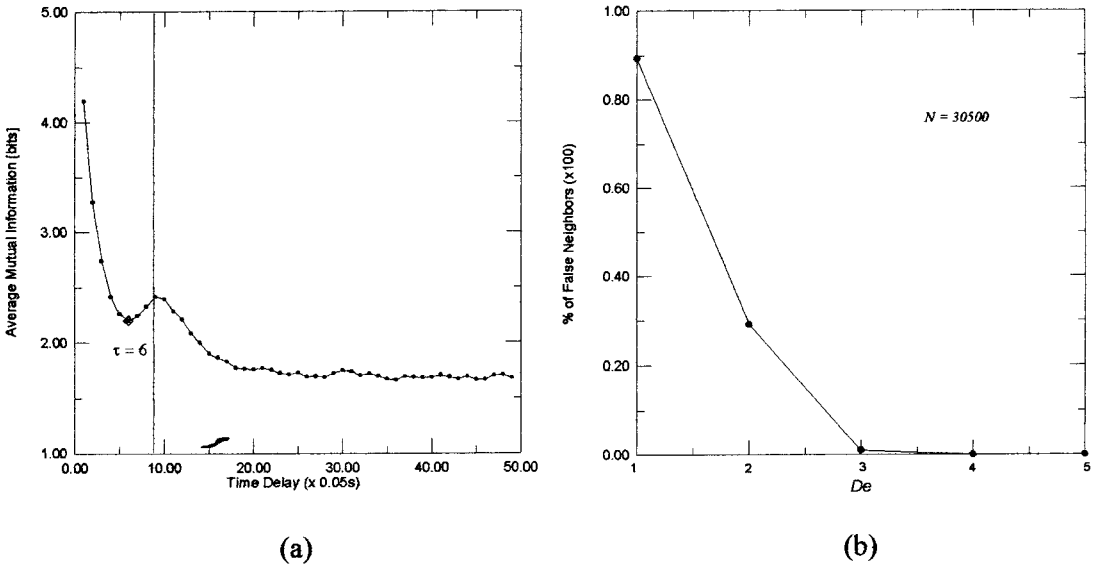

Figure 12. Delay parameters associated with chaotic signal. (a) Average mutual information *versus* τ; (b) percentage of false neighbors *versus* D_e.

5.2. Dynamical Invariants

Even though the system response presents a chaotic-like characteristic, it is important to assure this conclusion with the determination of dynamical invariants. At first, Lyapunov exponents are focused. Employing algorithms due to Kantz [11] and due to Rosenstein et al. [12] and regarding the Poincaré map signal, it is possible to estimate the maximum Lyapunov exponent. With this aim, the following parameters need to be conceived: $\varepsilon = 1.6$ and $D_e = 6, 9, 12$. It should be emphasized that the value of ε is the same to the one employed in the analysis of periodic signal, discussed in the preceding section. This value is defined from the 'calibration' of the algorithm and allows one to analyze different signals with the same parameters. Hence, it is possible to distinguish different kinds of motion.

The curve $S(\delta)$ *versus* δ, predicted by both algorithms, are presented in Figure 15. These curves present a linear range, which tends to reach a stabilized value. The slope of the curve in this linear range estimates the maximum Lyapunov exponent and may be computed employing a linear regression. Hence, the algorithm due to Kantz [11] furnishes $\lambda = 0.177 \pm 0.024$ while the algorithm due to Rosenstein et al. [12] furnishes $\lambda = 0.153 \pm 0.010$. As expected, the system presents a positive exponent. Here, in contrast with the periodic signal analysis, both algorithms are capable to identify chaotic behavior.

A further dynamical invariant may be useful to analyze the chaotic signal: attractor dimension. The continuous signal is regarded to determine the correlation dimension employing the algorithm due to Hegger et al. [23]. The correlation dimension for different values of embedding dimension is presented in Figure 16. The slope of the linear range in Figure 16a is related to the position of the horizontal range in Figure 16b and represents the value obtained for the correlation dimension. The first point arising to this result is that the linear (horizontal) range is greater than the one presented for the periodic signal. After a linear regression, the value estimated belongs to the range 2.20 to 2.77. This range does not include integer numbers, allowing one to identify the chaotic motion. Notice, however, that the attrac-

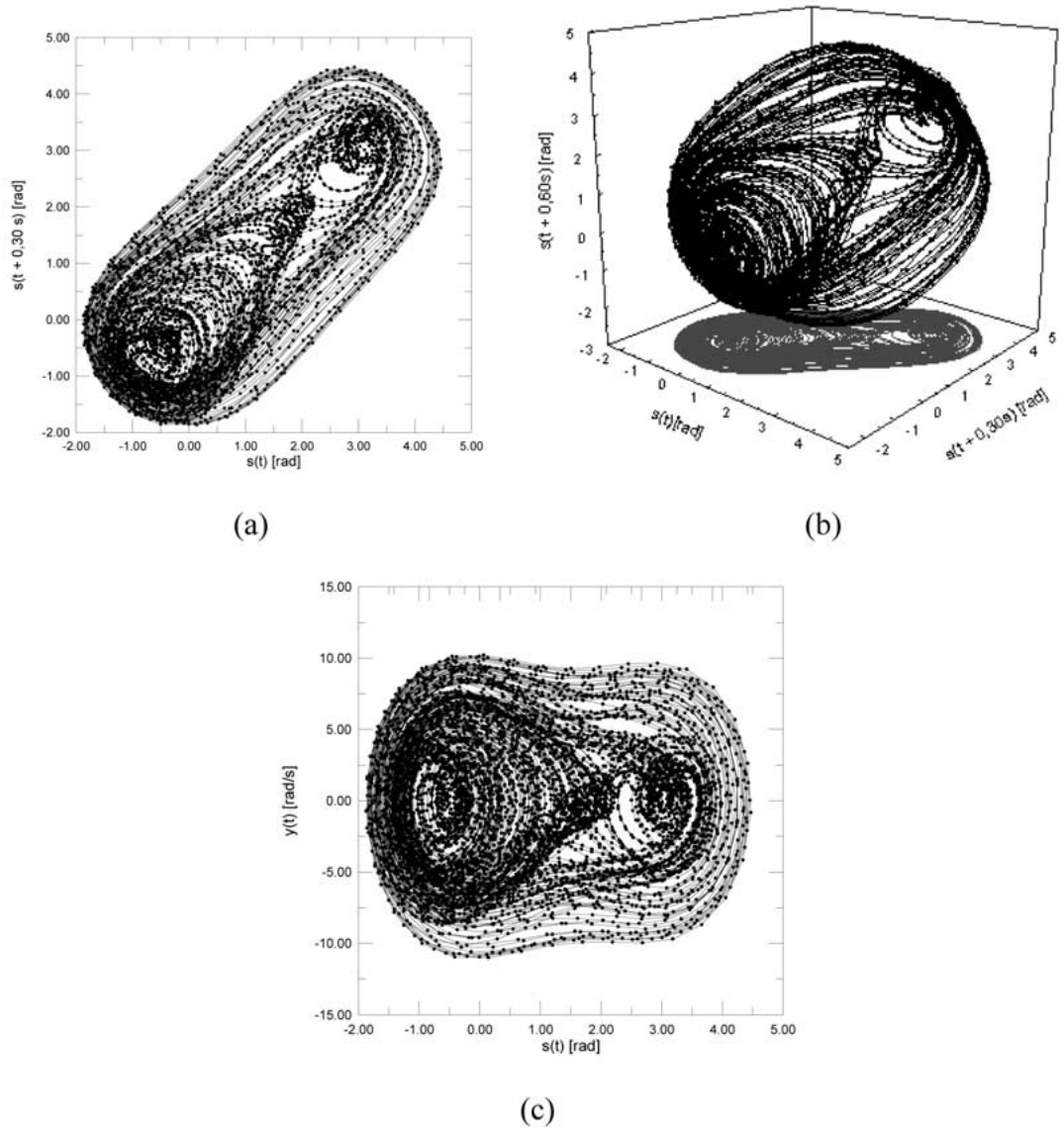

Figure 13. State space associated with chaotic signal. (a) Reconstructed, 2-Dim; (b) reconstructed, 3-Dim; (c) real.

tor dimension present difficulties to identify periodic motion and therefore, it is difficult to distinguish periodic and chaotic signals.

6. Conclusions

This contribution reports on the analysis of time series obtained from an experimental nonlinear pendulum. State space reconstruction is done employing the method of delay coordinates. Delay parameters are estimated with the average mutual information method to determine time delay and the false nearest neighbors method to estimate embedding dimension. Both methods present no noise sensitivity. A procedure to construct the Poincaré map is developed

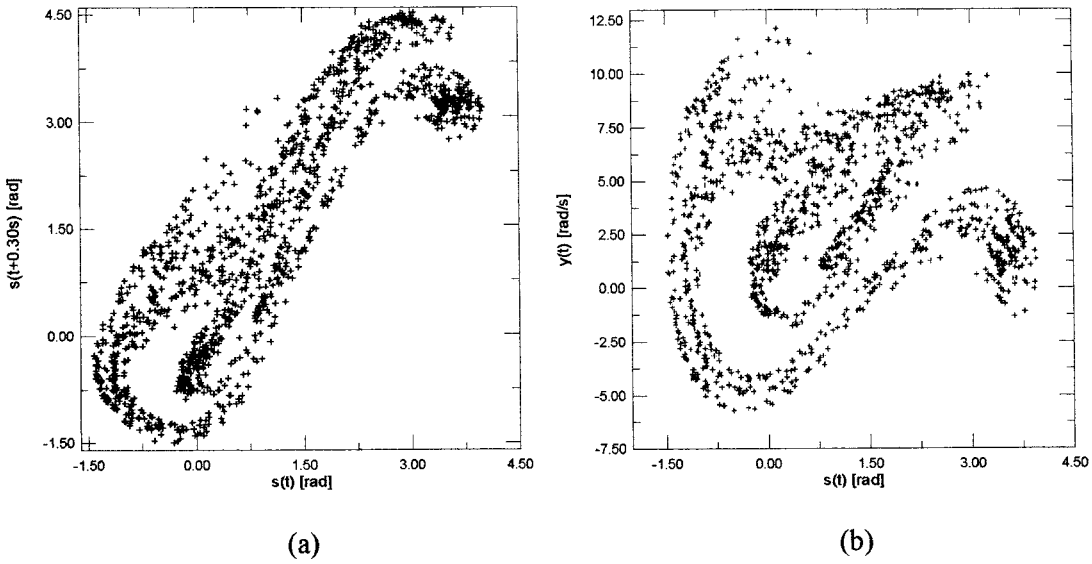

Figure 14. Poincaré map of chaotic signal: (a) reconstructed; (b) real.

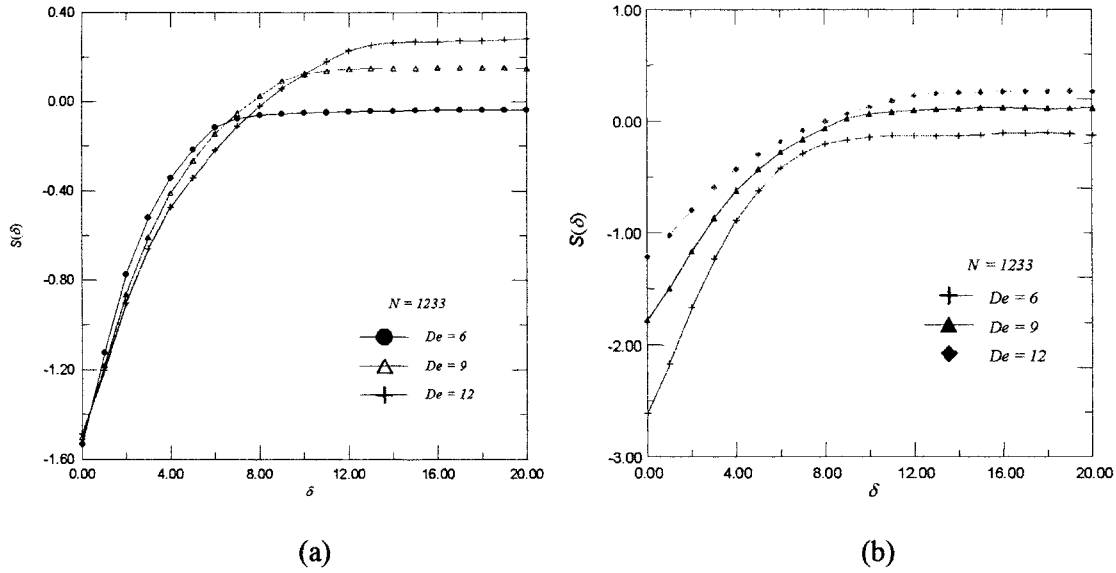

Figure 15. Lyapunov exponents associated with chaotic signal: $S(\delta)$ curves. (a) Kantz; (b) Rosenstein et al.

and presents good results. The FFT analysis allows one to identify chaos in this physical system, however, it is necessary to evaluate dynamical invariants to assure this conclusion. Lyapunov exponents and attractor dimension are used with this aim. Lyapunov exponents are calculated employing the algorithms due to Kantz and due to Rosenstein et al. After performing the proposed calibration procedure, the Kantz algorithm allows one to establish a difference between periodic and chaotic motion. The algorithm due to Rosenstein et al., on the other hand, does not present good results for periodic motion. Concerning the attractor dimension, the algorithm due to Hegger et al. is employed to estimate the correlation dimension. It should be noted that this is not an efficient tool to identify periodic signals. The authors agree

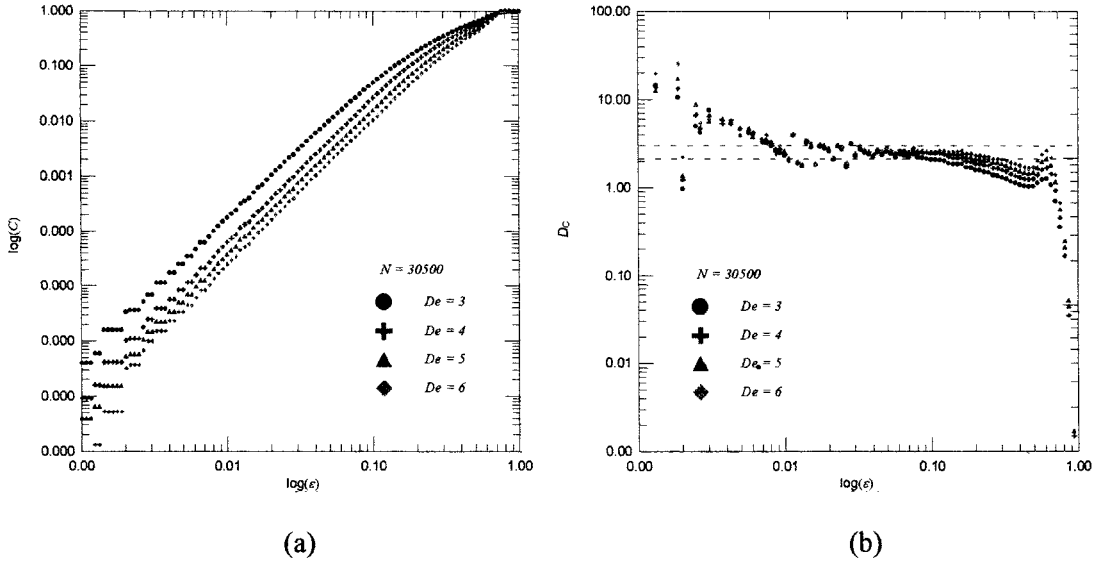

Figure 16. Lyapunov exponents associated with chaotic signal: $S(\delta)$ curves. (a) Kantz; (b) Rosenstein et al.

that this contribution show that it is possible to distinguish periodic and chaotic time series obtained from an experimental set up without employing any kind of filters. Other dynamical systems must be analyzed in order to validate the present conclusions, however one believes that the procedures employed here can be applied to any system response.

Acknowledgment

The authors acknowledge the support of the Brazilian Research Council (CNPq).

References

1. Ogata, S., Iwayama, T., and Terachi, S., 'Effect of system noise on chaotic behavior in Rossler type nonlinear system', *International Journal of Bifurcation and Chaos* **7**, 1997, 2872–2879.
2. Abarbanel, H., Brown, R., Sidorowich, J. J., and Tsimring, L. Sh., 'The analysis of observed chaotic in physical systems', *Reviews of Modern Physics* **65**, 1993, 1331–1392.
3. Kostelich, E. J. and Schreiber, T., 'Noise reduction in chaotic time-series data: A survey of common methods', *Physics Review E* **48**, 1993, 1752–1763.
4. Elsner, J. B., 'Predicting time-series using a neural network as a method of distinguishing chaos from noise', *Journal of Physics A – Mathematical and General* **25**, 1992, 843–850.
5. Derstine, M. W., Gibbs, H. M., Hopt, F. A., and Sanders, L. D., 'Distinguishing chaos from noise in an optically bistable system', *IEEE Journal on Quantum Electron* **21**, 1985, 1419–1422.
6. Packard, N. J., Crutchfield, J. P., Fromer, J. D., and Shaw, R. S., 'Geometry from a time-series', *Physical Review Letters* **45**, 1980, 712–716.
7. Takens, F., 'Detecting strange attractors in turbulence', in D. Rand and L.-S. Young (eds.), Lecture Notes in Mathematics, Vol. 898, Springer-Verlag, Berlin, 1981, pp. 366–381.
8. Broomhead, D. S. and King, G. P., 'Extracting qualitative dynamics from experimental data', *Physica D* **20**, 1986, 217–236.
9. Ruelle, D., 'Ergotic theory of differentiable dynamical systems', *Mathématique of the Institut des Hautes Études Scientifiques* **5**, 1979, 27.

10. Wolf, A., Swift, J. B., Swinney, H. L., and Vastano, J. A., 'Determining Lyapunov exponents from a time series', *Physica D* **16**, 1985, 285–317.
11. Kantz, H., 'A robust method to estimate the maximal Lyapunov exponent of a time series', *Physics Letters A* **185**, 1994, 77–87.
12. Rosenstein, M. T., Collins, J. J., and De Luca, C. J., 'A practical method for calculating largest Lyapunov exponents from small data sets', *Physica D* **65**, 1993, 117–134.
13. Sano, M. and Sawada, Y., 'Measurement of the Lyapunov spectrum from a chaotic time series', *Physical Review Letters* **55**, 1985, 1082–1085.
14. Eckemann, J.-P., Kamphorst, S. O., Ruelle, D., and Ciliberto, S., 'Lyapunov exponents from time series', *Physical Review A* **34**, 1986, 4971–4979.
15. Brown, R., Bryant, P., and Abarbanel, H. D. I., 'Computing the Lyapunov spectrum of a dynamical system from an observed time series', *Physical Review A* **43**, 1991, 2787–2806.
16. Briggs, K., 'An improved method for estimating Lyapunov exponents of chaotic time series', *Physics Letters A* **151**, 1990, 27–32.
17. Kruel, Th.-M., Eiswirth, M., and Schneider, F. W., 'Computation of Lyapunov spectra: Effect of interactive noise and application to a chemical oscillator', *Physica D* **63**, 1993, 117–137.
18. Zeng, X., Eykholt, R., and Pielke, R. A., 'Estimating the Lyapunov exponent spectrum from short time series of low precision', *Physical Review Letters* **66**, 1991, 3229–3232.
19. Brown, R., 'Calculating Lyapunov exponents for short and/or noisy data sets', *Physical Review E* **47**, 1993, 3962–3969.
20. Ellner, S., Nychka, D. W., and Gallant, A. R., 'A program to estimate the dominant Lyapunov exponent of noisy nonlinear systems from time series data', Institute of Statistics Mimeo Series #2235, 1992.
21. Farmer, J. D., Ott, E., and Yorke, J. A., 'The dimension of chaotic attractors', *Physica D* **7**, 1983, 153–180.
22. Franca, L. F. P., 'Analysis of chaotic systems from time series: Application to nonlinear pendulum', M.Sc. Dissertation, Department of Mechanical and Materials Engineering, Military Institute of Engineering, 2000 [in Portuguese].
23. Franca, L. F. P. and Savi, M. A., 'On the time series determination of Lyapunov exponents applied to the nonlinear pendulum analysis', in *Nonlinear Dynamics, Chaos, Control and Their Applications to Engineering Sciences, ABCM* **5**, 2000, 356–366.
24. Franca, L. F. P. and Savi, M. A., 'Estimating fractal dimension from time series: Case study of nonlinear pendulum', *Nonlinear Dynamics, Chaos, Control and Their Applications to Engineering Sciences, ABCM* **5**, 2000, 345–355.
25. Hegger, R., Kantz, H., and Schreiber, T., 'Practical implementation of nonlinear time series methods: The Tisean package', *Chaos* **9**, 1999, 413–435.
26. Kantz, H. and Schreiber, T., *Nonlinear Time Series Analysis*, Cambridge University Press, Cambridge, 1997.
27. Abarbanel, H. D. I., Gilpin, M. E., and Rotenberg, M., *Analysis of Observed Chaotic Data*, Springer-Verlag, Berlin, 1998.
28. Nayfeh, A. H. and Balachandran, B., *Applied Nonlinear Dynamics: Analytical, Computational, and Experimental Methods*, Wiley, New York, 1995.
29. Mullin, T., *The Nature of Chaos*, Oxford Press, Oxford, 1993.
30. Moon, F. C., *Chaotic and Fractal Dynamics*, Wiley, New York, 1992.
31. Box, G. G. P., Jenkins, G. M., and Reinsel, G. C., *Time Series Analysis*, Prentice Hall, Englewood Cliffs, NJ, 1994.
32. Fraser, A. M. and Swinney, H. L., 'Independent coordinates for strange attractors from mutual information', *Physical Review A* **33**, 1986, 1134–1140.
33. Grassberger, P. and Procaccia, I., 'Measuring the strangeness of strange attractors', *Physica D* **9**, 1983, 186.
34. Kennel, M. B., Brown, R., and Abarbanel, H. D. I., 'Determining embedding dimension from phase-space reconstruction using a geometrical construction', *Physical Review A 25*, 1992, 3403–3411.
35. Kaplan, D. T. and Glass, L., 'Direct test for determinism in a time-series', *Physical Review Letters* **68**, 1992, 427–430.
36. Cao, L., 'Practical method for determining the minimum embedding dimension of a scalar time series', *Physica D* **110**, 1997, 43.
37. Kennel, M. B. and Abarbanel, H. D. I., 'False neighbors and false strands: A reliable minimum embedding dimension', INLS Preprint, 1994.

38. Theiler, J., 'Estimating fractal dimension', *Journal of Optical Society of America* **7**, 1990, 1055–1073.
39. Takens, F., 'Invariants related to dimension and entropy', in *13º Colóquio Brasileiro de Matemática – IMPA*, 1983.
40. Meirovitch, L., *Elements of Vibration Analysis*, McGraw-Hill, New York, 1986.